NASA/TM—2004–213552

A "Kane's Dynamics" Model for the Active Rack Isolation System

Part Two: Nonlinear Model Development, Verification, and Simplification

G.S. Beech
Marshall Space Flight Center, Marshall Space Flight Center, Alabama

R.D. Hampton
United States Military Academy, West Point, New York

J.K. Rupert
Dynetics, Inc., Huntsville, Alabama

November 2004

The NASA STI Program Office…in Profile

Since its founding, NASA has been dedicated to the advancement of aeronautics and space science. The NASA Scientific and Technical Information (STI) Program Office plays a key part in helping NASA maintain this important role.

The NASA STI Program Office is operated by Langley Research Center, the lead center for NASA's scientific and technical information. The NASA STI Program Office provides access to the NASA STI Database, the largest collection of aeronautical and space science STI in the world. The Program Office is also NASA's institutional mechanism for disseminating the results of its research and development activities. These results are published by NASA in the NASA STI Report Series, which includes the following report types:

- TECHNICAL PUBLICATION. Reports of completed research or a major significant phase of research that present the results of NASA programs and include extensive data or theoretical analysis. Includes compilations of significant scientific and technical data and information deemed to be of continuing reference value. NASA's counterpart of peer-reviewed formal professional papers but has less stringent limitations on manuscript length and extent of graphic presentations.

- TECHNICAL MEMORANDUM. Scientific and technical findings that are preliminary or of specialized interest, e.g., quick release reports, working papers, and bibliographies that contain minimal annotation. Does not contain extensive analysis.

- CONTRACTOR REPORT. Scientific and technical findings by NASA-sponsored contractors and grantees.

- CONFERENCE PUBLICATION. Collected papers from scientific and technical conferences, symposia, seminars, or other meetings sponsored or cosponsored by NASA.

- SPECIAL PUBLICATION. Scientific, technical, or historical information from NASA programs, projects, and mission, often concerned with subjects having substantial public interest.

- TECHNICAL TRANSLATION. English-language translations of foreign scientific and technical material pertinent to NASA's mission.

Specialized services that complement the STI Program Office's diverse offerings include creating custom thesauri, building customized databases, organizing and publishing research results…even providing videos.

For more information about the NASA STI Program Office, see the following:

- Access the NASA STI Program Home Page at ***http://www.sti.nasa.gov***

- E-mail your question via the Internet to help@sti.nasa.gov

- Fax your question to the NASA Access Help Desk at 301–621–0134

- Telephone the NASA Access Help Desk at 301–621–0390

- Write to:
  NASA Access Help Desk
  NASA Center for AeroSpace Information
  7121 Standard Drive
  Hanover, MD 21076–1320
  301–621–0390

NASA/TM—2004–213552

A "Kane's Dynamics" Model for the Active Rack Isolation System

Part Two: Nonlinear Model Development, Verification, and Simplification

G.S. Beech
Marshall Space Flight Center, Marshall Space Flight Center, Alabama

R.D. Hampton
United States Military Academy, West Point, New York

J.K. Rupert
Dynetics, Inc., Huntsville, Alabama

National Aeronautics and
Space Administration

Marshall Space Flight Center • MSFC, Alabama 35812

November 2004

TRADEMARKS

Trade names and trademarks are used in this report for identification only. This usage does not constitute an official endorsement, either expressed or implied, by the National Aeronautics and Space Administration.

Available from:

NASA Center for AeroSpace Information
7121 Standard Drive
Hanover, MD 21076–1320
301–621–0390

National Technical Information Service
5285 Port Royal Road
Springfield, VA 22161
703–487–4650

TABLE OF CONTENTS

LIST OF FIGURES

LIST OF ACRONYMS AND SYMBOLS

ARIS	active rack isolation system
CAD	computer-aided design
COTS	commercial off-the-shelf
ISPR	international standard payload rack
ISS	*International Space Station*
TM	Technical Memorandum

NOMENCLATURE

`A_B_C>`	accelleration vector of arbitrary point `B` relative to arbitrary point `C`
`ALF_B_C>`	angular accelleration of arbitrary point `B` relative to arbitrary point `C`
A_{rs}	constraint equation scalar
`B`	arbitrary point
`C`	arbitrary point
F_r^*	system holonomic generalized inertia force for the *r*th generalized speed
$\tilde{F}_r^*$	system nonholonomic generalized inertia force for the *r*th generalized speed
F_s^*	generalized inertia force for *s*
i	index variable
n	variable
`P_B_C>`	position vector from arbitrary point `B` to arbitrary point `C`
`Q`	angle; rotation
r	index variable
$\tilde{S}$	total dynamic system (flotor, stator, actuator, and umbilicals)
s	index variable
u_r	dependent generalized speed
u_s	independent generalized speed
`V_B_C>`	velocity vector of arbitrary point `B` relative to arbitrary point `C`
`W_B_C>`	angular velocity of arbitrary point `B` relative to arbitrary point `C`

NOMENCLATURE (Continued)

X	arbitrary rigid body
Y	arbitrary rigid body
θ	angle

TECHNICAL MEMORANDUM

A "KANE'S DYNAMICS" MODEL FOR THE ACTIVE RACK ISOLATION SYSTEM

PART TWO: NONLINEAR MODEL DEVELOPMENT, VERIFICATION, AND SIMPLIFICATION

1. INTRODUCTION

In part one of this series, NASA/TM—2001–211063, a high-fidelity, linearized, analytical model of the active rack isolation system (ARIS) was derived using traditional, hand-calculation methods.[1] The model was developed directly, using Kane's method, without intermediate development of a full nonlinear model.[2,3] This Technical Memorandum (TM), part two, presents four computer-based, numerical models of ARIS, one of which is purely kinematical, and the remaining three, dynamical. These numerical models are used collectively to verify the linearized analytical model developed in part one.

The kinematical model uses high-fidelity computer-aided design (CAD) models and contains 17 rigid bodies and 48 degrees of freedom. It uses specified positions of actuator number 1, and ARIS geometry, to predict the configurations of the remaining seven actuators.

The three dynamical models are a simple truth model, a full nonlinear rigid-body model without umbilicals, and a corresponding linearized rigid-body model. The first dynamical model represents the system dynamics of an international standard payload rack (ISPR) in zero gravity with characteristic mass properties but without any actuators; it is used as a truth model, providing a benchmark for comparison purposes. The second dynamical model represents the full nonlinear system dynamics of an ARIS-outfitted ISPR. The actuator spring constants in the nonlinear model are first reduced, from nominal to negligible levels, for comparisons against the truth model using a set of test inputs. The actuator spring constants are then increased to moderate levels, to provide a more realistic representation of the system dynamics. The third dynamical model is a numerical model that has been linearized from the nonlinear model; it is a numerical representation of the linearized analytical model presented in part one. The input responses of this linearized model are compared to those of the nonlinear model. These comparisons confirm that the former, like the latter, accurately represents the physics of the system for ISPR motions within operational limits.

Once the three dynamical models have been run and compared, the kinematical model is used for visualization. The kinematical model drives a CAD representation of the ARIS config uration for specified times during the simulation. The result is a clear, visual representation of dynamical-model predictions of the configuration for the entire system at the various, arbitrary stages during the simulation.

2. DESCRIPTION OF SOFTWARE

The development and verification of the dynamical models were accomplished using two commercial-off-the-shelf (COTS) software tools: OnLine Dynamics' Autolev™ and DELMIA's® (formerly DENEB Robotics') ENVISION.[3–5]

ENVISION is a robotics software package developed for the automotive industry and employs three-dimensional CAD models to facilitate both forward and inverse kinematics analyses. Once CAD models of all of the rigid bodies of ARIS have been translated into ENVISION, coordinate systems representing the attachment locations are added. Then, in a parent-child fashion, from the CAD models, each ARIS actuator is built, and an algorithm for an inverse kinematics solution is applied to each. Next, all of the actuators, the *International Space Station* (*ISS*), and ISPR are appropriately combined, and the system is activated in a common CAD environment.

At this point, a user can specify the configuration of a single input actuator, and the remain ing seven actuators are forced to their unique configurations as determined by ENVISION's inverse kinematics algorithm and the constraints of the system. The configuration information for each of the actuators can then be compared to the corresponding configuration indicated by an Autolev simulation.

Autolev is a DOS-based interpreter that is designed, in general, to solve vector-based mathematical problems and, in particular, solve dynamics problems using Kane's method. Because Autolev is an interpreter, all of the commands entered for a particular session are stored in memory. A user can easily develop a text file containing the commands for a particular session. These files can be read by Autolev as if the commands had been entered manually.

The output from Autolev is a C program. This program when compiled, linked, and run, creates a DOS-executable file that, in turn, creates a data file of the specified output for a given simulation run. These automatically generated files are not included in this TM since they are very long and not easy to follow. Most of the descriptions in this TM illustrate the application of Autolev to the ARIS problem. There is a close correlation between the methods for the development of the closed-form analytical ARIS model and the Autolev model because both use Kane's method.

3. TRUTH MODEL

The first Autolev model represents the system dynamics of an ISPR in zero gravity with characteristic mass properties but without any actuators. Developed in Autolev, this model tracks the response in translation and rotation of the ISPR center of mass, as test forces are applied at various points on ISPR. The coordinates used in this model map the translation along and rotation about the x-, y-, and z-axes.

This model serves as a baseline for the comparison of other, more complex models, primarily because hardware validation would require resources beyond those currently available. One positive aspect of this model is that it is very simple so that its results are easily reproduced using various techniques. A limitation of this model is that it is useful only when the dynamical effects of the actuators are negligible. This requirement means, first, that the torsional springs at the lower and upper stingers and cross flexures must have a negligible stiffness, and second, the actuators must not reach full extension.

The actuator spring constants are easily changed to negligible levels. This is accomplished by specifying very small values for the spring constants in the code. The full-extension constraints only come into play when the actuators would otherwise extend beyond their physical limitations. In the actual hardware, the ISPR displacements from the home position are limited by a snubber system. However, in the Autolev model, there is no such system, so the motion must be limited by the disturbance input.

4. NONLINEAR ACTIVE RACK ISOLATION SYSTEM MODEL

Kane's method was used to develop both the linearized analytical model, presented in part one of this series, and the corresponding Autolev model discussed in this TM.[1–3] Most of the developmental steps outlined in part one are implemented specifically by corresponding commands in Autolev, and in a few cases, Autolev automates several steps with a single command. A copy of the text file that represents the nonlinear ARIS model is given in *A High Fidelity Model for the Active Rack Isolation System.*[6]

4.1 Rotation Matrices

Using Autolev notation, let the `Aij>` coordinate system rotate, relative to the `Fij>` coordinate system, through positive angle `Q(1+6n), (n=0,…,7)` about the `Fi3>` axis. Similarly, let the orientation of the `Aij>` coordinate system, relative to the `Pij>` coordinate system, be described by consecutive positive rotations: `Q(2+6n)` about the `Pi1>` axis and `Q(3+6n)` about the moved `3` axis. Also, let the orientation of the `Pij>` coordinate system, relative to the `Sij>` coordinate system, be described by consecutive positive rotations: `Q(4+6n)` about the `Si3>` axis, `Q(5+6n)` about the moved `2` axis, and `Q(6+6n)` about the moved `1` axis.

As entered into Autolev, the rotation matrices among the several coordinate systems for the first actuator assembly are

```
SIMPROT(Sa,Ra,3,Q4) ,                    (1)

SIMPROT(Sa,Ra,2,Q5) ,                    (2)

SIMPROT(Qa,Pa,2,Q6) ,                    (3)

SIMPROT(Pa,Ta,2,Q2) ,                    (4)

SIMPROT(Ta,Aa,2,Q3) ,                    (5)
```

and

```
SIMPROT(Fa,Aa,2,Q1) .                    (6)
```

Define the rotation matrix between each of the eight, stator-fixed coordinate systems, `Sij>`, and the single, stator-fixed, reference coordinate system, `Sj>`. Measurements from the ENVISION model for the first actuator show that

```
Sa_S=[0,-0.7071,0.7071;0,0.7071,0.7071;-1,0,0] ,          (7)
```

where the commas separate elements within a row and the semicolons separate the rows.

Next, define the rotation matrix between each of the eight, flotor-fixed coordinate systems, `Fij>`, and the single, flotor-fixed, reference coordinate system, `Fj>`. For the first actuator (from the ENVISION model),

```
F_Fa=[0,0,1;0.86603,-0.5,0;0.5,0.8663,0] .
```
(8)

Note that the nomenclature, `F_Fa`, represents the rotation from the `Fa>` system, fixed on the ISPR at the cross flexure to the `F>` system, fixed on the flotor at the center of mass.

4.2 Generalized Coordinates

The 48 angles, `Qj(j=1,…,48)`, are the generalized coordinates of the system. For the *i*th actuator, the six associated generalized coordinates are as follows:

- `Q(1+6n)(n=0,…,7)` is the angle at the cross flexure of the ith actuator.
- `Q(2+6n)` and `Q(3+6n)` are the angles at the upper stinger.
- `Q(4+6n),Q(5+6n),` and `Q(6+6n)` are the angles at the lower stinger.

4.3 Generalized Speeds

Define generalized speeds `Uj(j=1…48)` for the system as the time rates of change of the independent generalized coordinates of $\tilde{S}$ in the inertial reference frame:

```
Uj=Qj´(j=1...6) .
```
(9)

4.4 Angular Velocities of the Reference Frames and Rigid Bodies

Designate the reference frames corresponding to the stator, the *i*th push rod, the *i*th arm, and the flotor by the symbols `Sj>`, `Pij>`, `Aij>`, and `Fj>`, respectively. Let `Sij>` and `Fij>` represent, respectively, the coordinate systems in `Sj>` and `Fj>` located at the respective points `Oi` and `F1i`.

Two intermediate reference frames were introduced previously to permit describing the angular velocity of each pushrod relative to the stator. Designate those intermediate frames corresponding to the ith actuator assembly by `Rij>` and `Qij>`. Another intermediate reference frame was previously introduced between frames `Pij>` and `Aij>`; designate this by `Tij>`.

With the expression for angular velocity denoted `W_Aa_Fa>` corresponding to the angular velocity of `Aaj>` relative to `Faj>`, the following expressions represent the angular velocities through the first actuator in Autolev:

```
W_S_N>=0> ,
```
(10)

```
W_Sa_S>=0> ,
```
(11)

```
W_Ra_Sa>=U4*Sa3>
```
(12)

```
W_Qa_Sa>=U4*Sa3>+U5*Ra2> ,                                          (13)

W_Pa_Sa>=U4*Sa3>+U5*Ra2>+U6*Qa1> ,                                  (14)

W_Ta_Sa>=U4*Sa3>+U5*Ra2>+U6*Qa1>+U2*Pa1> ,                          (15)

W_Aa_Sa>=U4*Sa3>+U5*Ra2>+U6*Qa1>+U2*Pa1>+U3*Ta3> ,                  (16)

W_Fa_Sa>=U4*Sa3>+U5*Ra2>+U6*Qa1>
+U2*Pa1>+U3*Ta3>-U1*Fa> ,                                          (17)

W_Aa_Pa>=U2*Pa2>+U3*Ta3> ,                                         (18)

W_Fa_Aa>=-U1*Fa3> ,                                                (19)
```

and

```
W_F_Fa>=0> .                                                       (20)
```

4.5 Angular Accelerations of the Reference Frames and Rigid Bodies

The designation `ALF_X_Y>` represents the angular acceleration of the coordinate system or rigid body, `X`, with respect to the coordinate system or rigid body, `Y`. They are calculated as the time derivatives of the angular velocities above, using the Autolev commands

```
ALF_S_N>=0> ,                                                      (21)

ALF_Sa_S>=0> ,                                                     (22)

ALF_Ra_Sa>=DT(W_Ra_Sa>,Sa) ,                                       (23)

ALF_Qa_Sa>=DT(W_Qa_Sa>,Sa) ,                                       (24)

ALF_Pa_Sa>=DT(W_Pa_Sa>,Sa) ,                                       (25)

ALF_Ta_Sa>=DT(W_Ta_Sa>,Sa) ,                                       (26)

ALF_Aa_Sa>=DT(W_Aa_Sa>,Sa) ,                                       (27)

ALF_Fa_Sa>=DT(W_Fa_Sa>,Sa) ,                                       (28)

ALF_Aa_Pa>=DT(W_Aa_Pa>,Sa) ,                                       (29)

ALF_Fa_Aa>=DT(W_Fa_Aa>,Sa) ,                                       (30)
```

and

```
ALF_F_Fa>=0> .                                                    (31)
```

4.6 Velocities of the Centers of Mass for the Rigid Bodies

Represent by `P_B_C>` the position vector from arbitrary point `B` to arbitrary point `C`. Define the following position vectors for the first actuator (and similarly for the remaining seven), as measured from the ENVISION model:

```
P_Oa_A2a>=1.375*Pa2> ,                                            (32)

P_Oa_Pao>=0.6875*Pa2> ,                                           (33)

P_A2a_F1a>=-0.25*Aa1> ,                                           (34)

P_A2a_Aao>=0.2375*Aa1>+0.07917*Aa2> ,                             (35)
```

and

```
P_F1a_Fo>=2.122*Fa1>+1.578*Fa2>-1.494*Fa3> .                      (36)
```

The first derivatives of the appropriate position vectors, under the stated assumptions, yield expressions for the velocities of the centers of mass for the 17 rigid bodies. The Autolev commands that follow are used to generate expressions for the nonlinear velocities of the centers of mass for the pushrod, arm, and flotor; i.e., ISPR, through the first actuator:

```
V_Oa_Sa>=0> ,                                                     (37)

V2PTS(Sa,Pa,Oa,A2a) ,                                             (38)

V2PTS(Sa,Pa,Oa,Pao) ,                                             (39)

V_Pao_N>=V_Pao_Sa> ,                                              (40)

V2PTS(Sa,Aa,A2a,F1a) ,                                            (41)

V_F1a_N>=V_F1a_Sa> ,                                              (42)

V2PTS(Sa,Aa,A2a,Aao) ,                                            (43)

V_Aao_N>=V_Aao_Sa> ,                                              (44)

V2PTS(Sa,Fa,F1a,Fo) ,                                             (45)
```

and

```
V_Fo_N>=V_Fo_Sa> .                                                (46)
```

4.7 Accelerations of the Centers of Mass for the Rigid Bodies

Taking the time derivatives of the respective linearized velocity vectors yields expressions for the linearized accelerations of the centers of mass for each rigid body. This is accomplished with the following Autolev commands for the first actuator and in a similar manner for the additional seven:

```
A_So_N>=0> ,                                    (49)

A_Oa_N>=0> ,                                    (50)

A2PTS(N,Pa,Oa,A2a) ,                            (51)

A2PTS(N,Pa,Oa,Pao) ,                            (52)

A2PTS(N,Aa,A2a,F1a) ,                           (53)

A2PTS(N,Aa,A2a,Aao) ,                           (54)
```

and

```
A2PTS(N,Fa,F1a,Fo) .                            (55)
```

4.8 Partial Velocities and Partial Angular Velocities

Partial velocities and partial angular velocities are required with Kane's method for determining the generalized active and generalized inertial forces. These calculations can be made explicitly by use of the Autolev `PARTIALS` command for a check of hand calculations. However, in the development of the Autolev model, the calculations can be performed automatically without the `PARTIALS` command by using the commands `FR()` and `FRSTAR()`. These commands calculate the generalized active and generalized inertial forces, respectively.

4.9 Generalized Active Forces

As mentioned in section 4.8, the generalized active forces and generalized inertia forces are calculated automatically by the `FR()` and `FRSTAR()` commands. Onorbit; i.e., neglecting the effects of gravity, the system is acted on by forces and moments due to the Lorentz coil, umbilical, and direct disturbance. Of these loads, only the forces and moments due to the actuator springs, and direct disturbances are considered.

4.10 Contributions Due to the Pushrods

The contributing loads on each pushrod are moments generated at the pertinent upper and lower stingers:

```
TORQUE(Pa,0.001*Q2*Pa1>+0.001*Q3*Ta3>)                    (56)
```

and

```
TORQUE(Pa,0.001*Q4*Sa3>+0.001*Q5*Ra2>+0.001*Q6*Qa1>) .    (57)
```

4.11 Contributions Due to the Actuator Arms

The forces and moments acting on the first actuator arm are due to the respective Lorentz coil, located at `A3a`; the flotor, through the first cross flexure; and the respective pushrod, through the upper stinger. Although the control input forces and moments are also contributing loads, they are not considered for the present Autolev models.

The remaining contributing loads are due to the flotor and pushrods. The reaction forces between these elements are noncontributing. The contributing loads are

```
TORQUE(Aa,0.001*Q1*Fa3>)                                  (58)
```

and

```
TORQUE(Aa,0.001*Q2*Pa1>+0.001*Q3*Ta3>) ,                  (59)
```

where the value, 0.001, denotes the cross-flexure stiffness (eq. (58)) and upper-stinger spring stiffness (eq. (59)) measured in lbf-in/rad. (Note the coupling between the control inputs and the generalized coordinates.)

4.12 Contributions Due to the Flotor

The actuators transmit loads to the flotor at the actuator cross flexures. These loads for the first actuators consist of a force applied at a point `F1a` and a moment exerted through the cross flexure. Since the force is noncontributing, it can be ignored in the analysis. The moment due to the cross-flexure spring is

```
TORQUE(F,0.001*Q1*Fa3>) ,                                 (60)
```

where 0.001 is the cross-flexure spring stiffness measured in lbf-in/rad. The loads for the other actuators can be considered analogously.

Unknown direct disturbance forces also act on the flotor. These can be represented as a force-moment pair, where the force is assumed to act through the flotor mass center, `Fo`. Let `FORCE(Fo,…)` and `TORQUE(F,…)` represent, together, this force-moment pair, where the ellipses indicate the magnitude and direction information, which must be supplied for an actual simulation run. Then the generalized-active-force contribution due to this pair could be determined explicitly, if desired, by the command

```
GAF ( ) =DOT(V_Fo_N>,FORCE(Fo,...) ) +DOT(W_F_N>,TORQUE(F,...) )  .   (61)
```

4.13 Generalized Inertial Forces

As with the generalized active forces, the generalized inertial forces are also calculated automatically by Autolev in response to the `FRSTAR()` command. Autolev uses the previously-calculated angular velocities and angular accelerations along with the user-defined inertial properties for these calculations.

The central principal moments of inertia of the first actuator arm are defined as follows (using the designation `Aa` to indicate actuator number 1):

```
INERTIA Aa,7e-5,7e-5,7e-5 .
```
(62)

Similarly, for the first pushrod:

```
INERTIA Pa,7e-4,7e-4,7e-4 .
```
(63)

The corresponding inertias for the remaining actuator arms and pushrods are defined analogously. These values for the actuator moments of inertia are reasonable approximations, and they can be modified as better data become available. The inertias for the ISPR and the *ISS* are entered respectively as

```
INERTIA F,66.8,166.8,71.5,-0.03,0.02,1.17 ,
```
(64)

and

```
INERTIA S,6875,36875,36875,-6,4,234 .
```
(65)

The centers of mass for the components are as entered in equations (33), (35), and (36). Again, once the mass properties have been defined, the generalized active forces are automatically calculated by Autolev in the course of evaluating `FRSTAR()`.

4.14 Constraint Equations

All together, there are a total of 54 constraint equations: 48 kinematical and 6 dynamical. Since the complete set of equations for a system with n generalized coordinates consists of $2n$ equations and since the ARIS system has 48 such coordinates, 42 more equations are needed to complete the set. These additional equations are the holonomic constraint equations (in nonholonomic form) for the dependent generalized speeds, `Ui,(i = 1,…,48)`.

Since the velocity of the flotor center of mass, `Fo`, is the same irrespective of the actuator path chosen for describing its position, a set of constraint equations can be written in vector form for the first two actuators:

```
DOT(V_Fo_Sa>,F1>)-DOT(V_Fo_Sb,F1>)=0 ,
```
(66)

```
DOT(V_Fo_Sa>,F2>)-DOT(V_Fo_Sb,F2>)=0 ,
```
(67)

and

```
DOT(V_Fo_Sa>,F3>)-DOT(V_Fo_Sb,F3>)=0 .
```
(68)

There are an additional 3 equations for each of the remaining 6 actuators for a total of 21 constraint equations; e.g., for the third actuator, one would substitute the lowercase "c" for "b" in equations (66)–(68).

Since the angular velocity of the flotor, F, is the same, irrespective of the actuator path chosen, another set of constraint equations can be written in vector form for the first two actuators:

```
DOT(W_F_Sa>,F1>)-DOT(W_F_Sb>,F1>)=0 ,
```
(69)

```
DOT(W_F_Sa>,F2>)-DOT(W_F_Sb>,F2>)=0 ,
```
(70)

and

```
DOT(W_F_Sa>,F3>)-DOT(W_F_Sb>,F3>)=0 .
```
(71)

Similarly, one can write equations that compare the flotor angular velocity through the first actuator with the flotor angular velocity through the third actuator (substituting "c" for "b" as above), and so forth. This process yields the final 21 constraint equations. To finish implementing these 42 relationships, Autolev uses the command

```
CONSTRAIN(DEPENDENT[U7,U8,U9,U10,U11,U12,U13,U14,U15,U16,
                    U17,U18,U19,U20,U21,U22,U23,U24,U25,
                    U26,U27,U28,U29,U30,U31,U32,U33,U34,
                    U35,U36,U37,U38,U39,U40,U41,U42,U43,
                    U44,U45,U46,U47,U48]) ,
```
(72)

After this final command has been executed, the 42 dependent generalized speeds are no longer used in the Autolev model.

5. COMPARISON BETWEEN NONLINEAR AND TRUTH MODELS

To compare the truth model and the nonlinear model, the cross-flexure stiffness and stinger-spring stiffness were set to negligible levels, 0.001 lbf-ft/rad (0.00021 lbf-in/deg). Various test inputs were applied at selected target points to compare these models. Two such test inputs were (1) a constant, 1-lb force with a constant direction relative to the ISPR, and (2) an oscillating force with an amplitude of 1 lb and an angular frequency of 0.2 rad/s. For the tests presented below, the target point was arbitrarily displaced 6 in per direction, `F1>`, `F2>`, and `F3>`, from the flotor center of mass. The direction of application for each force is along the `F1>` direction; i.e., along the ISPR x-axis.

The first comparison between the nonlinear and truth models (fig. 1) shows the response of each model to an oscillating input force applied directly to the ISPR. The respective model behaviors are very similar throughout the 10-s simulation. The differences between the two can be attributed to round-off errors in the fixed rotations between the *ISS*, ISPR and actuator-fixed coordinate systems, and some minimal effect due to the actuator springs. In this comparison, the actuators are not fully extended, so there are no noticeable effects from the constraint equations.

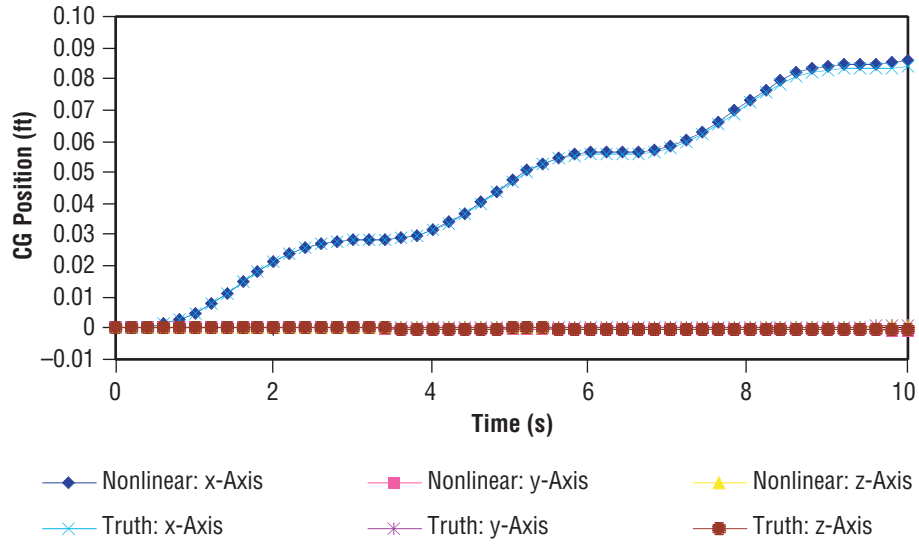

Figure 1. Comparison No. 1 between truth and nonlinear models.

The second comparison (fig. 2) shows the response of each model to a constant input force applied to the ISPR. In this model, the response of the nonlinear model tracks the response of the truth model for ≈4.4 s, or until the mass center has moved ≈3 in (0.25 ft). At this point, an actuator linkage is fully extended, which produces a jerk, and the motion reverses direction.

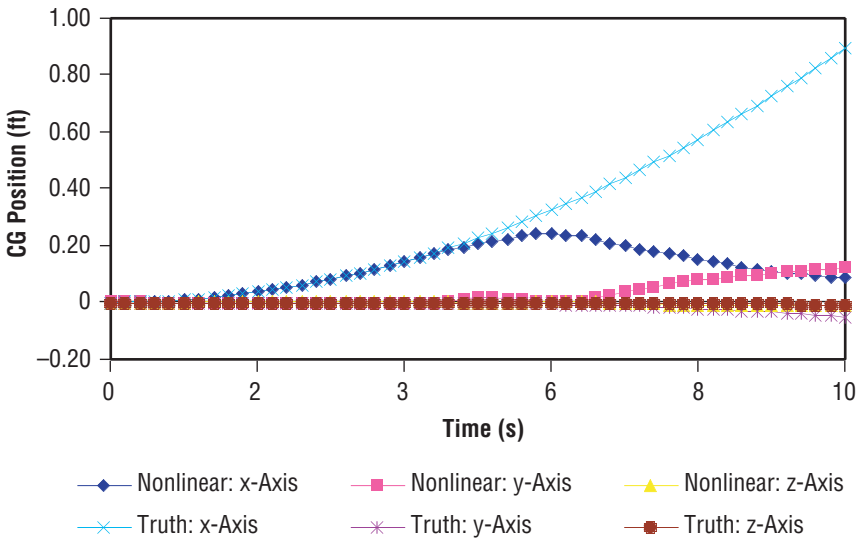

Figure 2. Comparison No. 2 between truth and nonlinear models.

This explanation for the behavior was further verified by the visualization afforded by the ENVISION model. At the time in the simulation when the ISPR center of gravity reversed direction; i.e., 4.4 s, the actuator configuration predicted by Autolev was recorded. That data were then entered into the ENVISION model, which clearly showed an actuator arm and pushrod having just reached full extension (fig. 3).

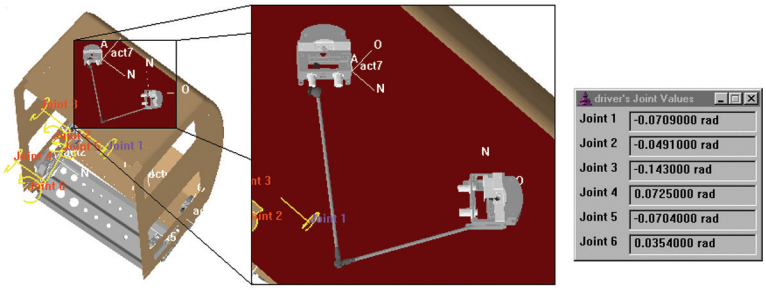

Figure 3. ENVISION visualization of ARIS actuators near full extension.

6. LINEARIZED ACTIVE RACK ISOLATION SYSTEM MODEL

With the full nonlinear model of ARIS completed, linearization is relatively easy using the Autolev system. The automatic linearization of the generalized active and generalized inertial forces is accomplished with the `AUTOTAYLOR` command. The arguments for `AUTOTAYLOR` describe the order of the terms of a Taylor-series expansion, here the zero and first order terms and the arguments about which the Taylor-series expansion is performed. For the first 10 generalized coordinates and generalized speeds,

```
AUTOTAYLOR(0:1,Q1,Q2,Q3,Q4,Q5,Q6,Q7,Q8,Q9,Q10) ,          (73)

AUTOTAYLOR(0:1,Q1',Q2',Q3',Q4',Q5',Q6',Q7',Q8',Q9',Q10') ,  (74)

AUTOTAYLOR(0:1,U1,U2,U3,U4,U5,U6,U7,U8,U9,U10) ,          (75)
```

and

```
AUTOTAYLOR(0:1,U1',U2',U3',U4',U5',U6',U7',U8',U9',U10') .  (76)
```

This is continued for the remaining 38 generalized speeds and generalized coordinates. The result is a linearized form of the ARIS dynamics.

7. COMPARISON BETWEEN LINEARIZED AND NONLINEAR MODELS

The small-angle theorem is based on a truncated Maclaurin-series expansion of the expressions for sine and cosine (about θ=0):

$$\sin\theta = \theta - \frac{\theta^3}{3} + \frac{\theta^5}{5} - \ldots \tag{77}$$

and

$$\cos\theta = 1 - \frac{\theta^2}{2} + \frac{\theta^4}{4} - \ldots \ . \tag{78}$$

Depending on the application, this approximation is accurate for values of θ less than ≈17°. In the present application, the constraint equations are most affected by the linearization, and values of θ less than ≈8° produce small-angle approximations that remain valid.

To ensure that the ISPR remains centered in its rattle space, and that the small-angle approximations remain valid, the spring stiffness at the cross flexure and upper and lower stingers were next increased to nominal levels. The spring rates are set to 1 lbf-ft/rad (0.21 lbf-in/deg). In figure 4, one can see how the effect of the increased actuator spring constants changes the ISPR response to the applied force. The ISPR motion in the case for the moderate actuator spring constants is relatively small compared to the ISPR motion when the actuator spring constants are negligible.

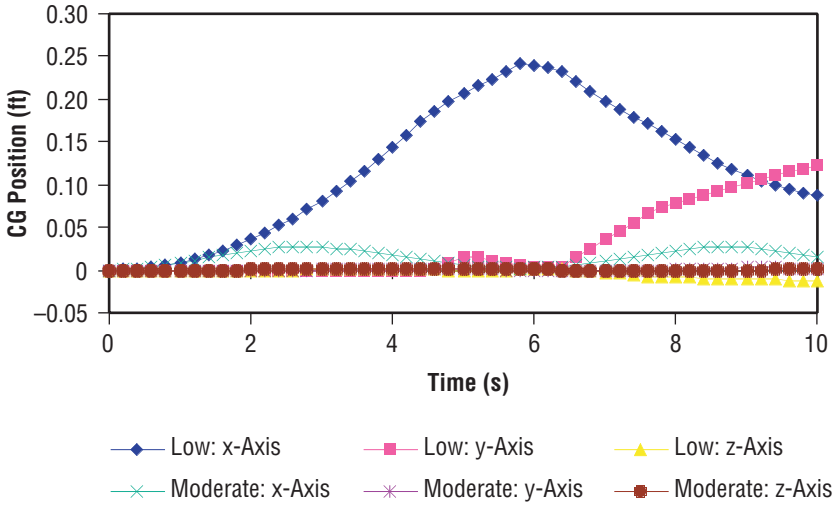

Figure 4. Low versus moderate actuator spring stiffness—response to constant test input.

Figure 5 shows the response measured in actuator number 1 angles when the spring constants are negligible and the ISPR is subjected to a constant input force. At ≈4.4 s, the actuator angles exceed the region bounded by the ±0.2 rad, where the constraint equations are valid. This point is further emphasized in figure 6, which shows that the linearized model has very good correspondence with the nonlinear model until the simulation reaches 4.4 s. After that, the linearized model fails because the constraint equations no longer hold.

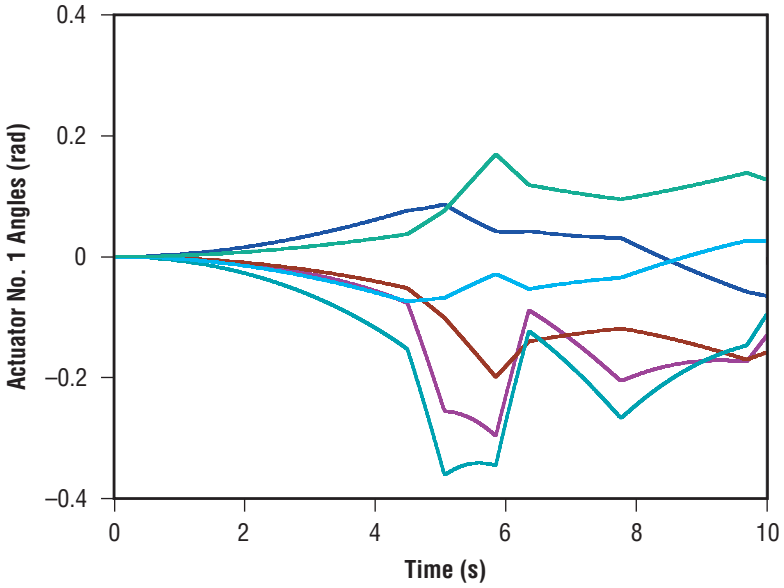

Figure 5. Actuator No. 1 angles relative to small-angle approximation (±0.2 rad)—low actuator spring rates.

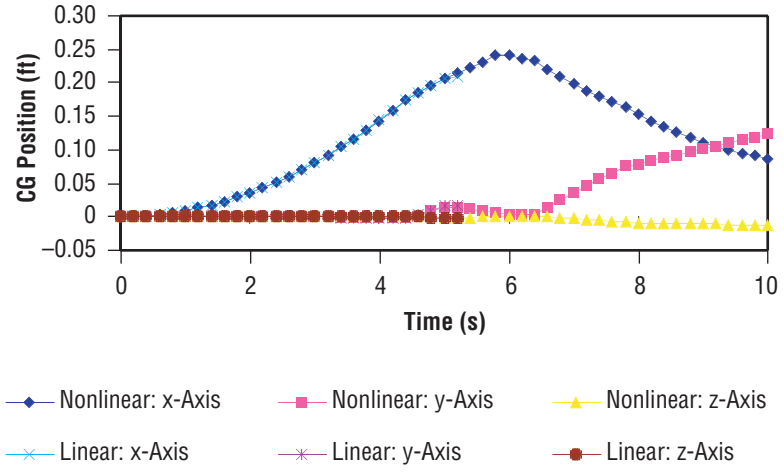

Figure 6. Linearized versus nonlinear model, low stiffness—response to direct, constant test input.

Figure 7 shows the response measured in actuator number 1 angles when the spring constants are increased to moderate levels (0.21 lbf-in/deg) and the ISPR is again subjected to a constant input force. In this case, the angles never exceed the region defined by ±0.2 rad. In fact, the angles for actuator number 1 never exceed ±0.1 rad. Figure 8 shows a comparison between the ISPR motion in the linearized and nonlinear models when the actuator spring constants are increased to moderate levels. There is a nearly exact match between these models.

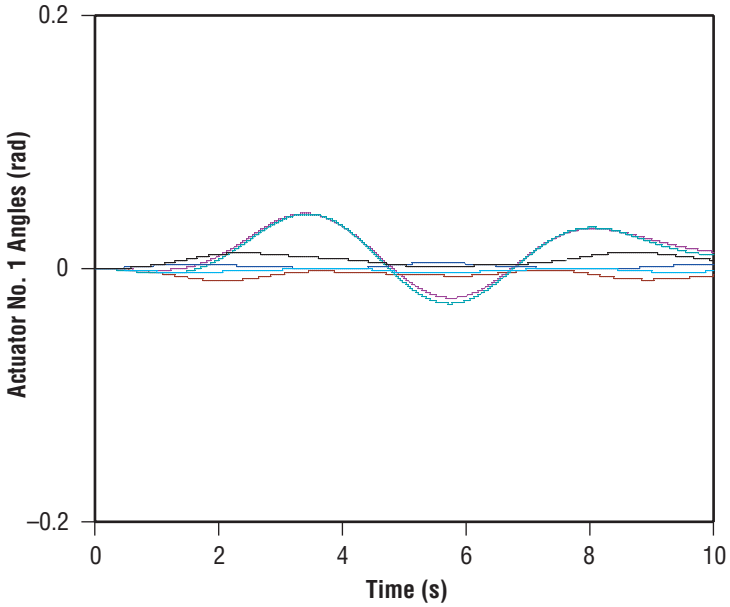

Figure 7. Actuator No. 1 angles relative to small-angle approximation (±0.2 rad)—moderate actuator spring rates.

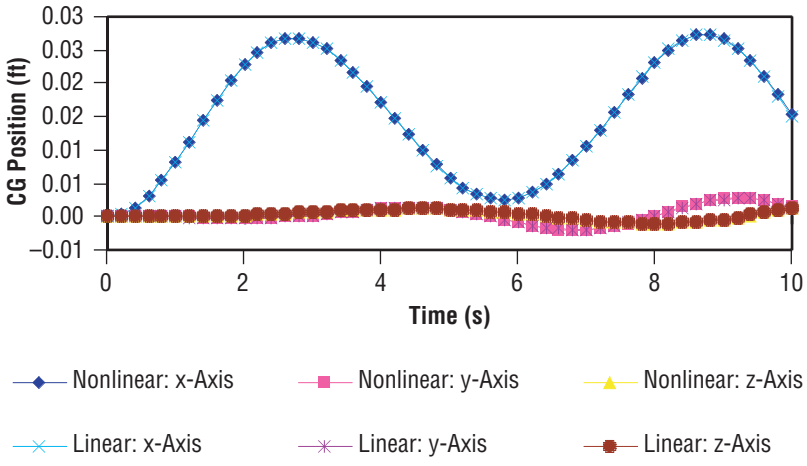

Figure 8. Linearized versus nonlinear model, moderate stiffness—response to direct, constant test input.

This important result shows that, for small angles, the linearized model very closely tracks the nonlinear model, which, in turn, closely tracks the truth model. With the actual hardware, the ISPR must remain near the center of its rattle space due to the snubber system (fig. 3). Further, the control system for ARIS is designed to keep the ISPR from even contacting the snubbers. Assuming that truth model, which is relatively simple, is correct, then the linearized model presented in part one is accurate within operational or rattle-space limits.

8. LINEARIZED REDUCED-MASS MODEL OF THE ACTIVE RACK ISOLOATION SYSTEM

A further simplification can be made by setting the mass properties (masses and inertias) of the actuator arms and pushrods to zero, while retaining those of the ISPR. The arms and pushrods represent 16 of the 17 bodies in the generalized inertia forces of the nonlinear and linearized models, but only about 1.5 percent of the mass of an ARIS-outfitted ISPR. By setting the mass properties of the arms and pushrods to zero, the number of expressions in the set of holonomic generalized inertial forces eq. (A–180) of part one of this TM series) is reduced by 288 (r =1,…, 48, i=1,…,16).[1] It was shown that dependent and independent generalized speeds, u_r and u_s, respectively, related as

$$u_r = \sum_{s=1}^{6} A_{rs} u_s \left(\text{for } r = 7,\ldots,6\right) \ . \tag{79}$$

The nonholonomic and holonomic generalized inertia forces, $\tilde{F}_r^*$ and F_r^*, respectively, relate as

$$\tilde{F}_r^* = F_r^* + \sum_{s=7}^{48} F_s^* A_{rs} \left(r = 1,...,6\right) \ . \tag{80}$$

Since Kane's method yields only as many dynamical equations as independent generalized speeds, removing these 288 expressions from the holonomic generalized inertial forces produces a net reduction of 1728 (6×288) terms in the final system equations.

Despite the great reduction in the number of terms in the generalized inertia forces, the simplified or reduced-mass dynamical equations maintain the integrity of the generalized active forces, including control and disturbance inputs, and the constraint equations. The final dynamical equations, therefore, are the same as those reported previously in part one, excluding the contributions to the generalized inertia forces from the arms and pushrods.[1]

9. COMPARISON BETWEEN LINEARIZED AND LINEARIZED REDUCED-MASS MODELS

Since the generalized inertia forces are the most complex expressions in the dynamical equation development, the omission of the 288 expressions for the arms and pushrods represents a substantial reduction in the overall size of the dynamical equations.[6] This simplification is made by simply setting the appropriate masses, moments, and products of inertia to zero in the Autolev code, and then recompiling the generated C program.

Figure 9 shows the response measured, in linear displacement of the ISPR center of mass, when the spring constants are increased to moderate levels (0.21 lbf-in/deg) and the ISPR is again subjected to a constant input force. From this plot, it is apparent that neglecting the mass properties of the arms and pushrods have little effect on the model's description of system behavior. This is as expected, for two reasons: (1) As noted previously, the masses of the arms and pushrods are relatively small in comparison to the overall mass of an ARIS-outfitted ISPR, and (2) Because the ARIS arms and pushrods are more closely linked to the (relatively fixed) space station than to the ISPR, the amplitudes of their displacements, velocities, and accelerations will be correspondingly smaller than those of the ISPR.

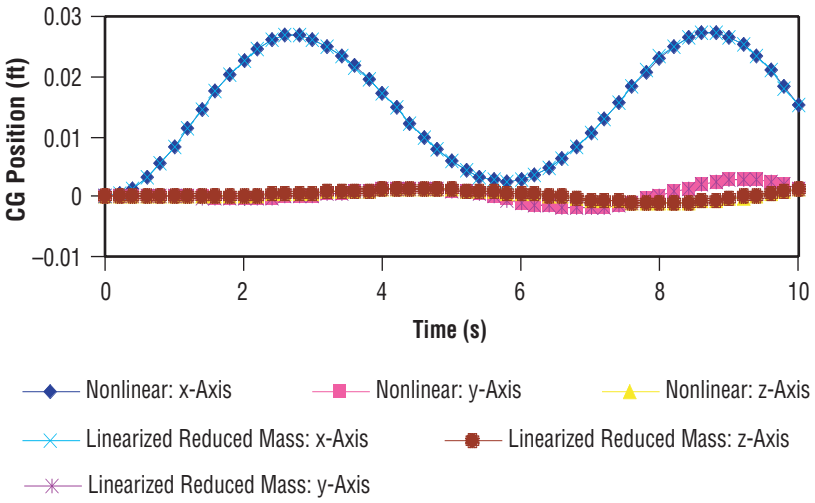

Figure 9. Linearized reduced mass versus nonlinear model, moderate stiffness—response to direct, constant test input.

10. CONCLUDING REMARKS

Part one of this series presented a high-fidelity, linearized, analytical model of ARIS suitable for controller design.[1] In this TM, part two, two COTS software packages were used to develop comparisons among nonlinear, linearized, and linearized reduced-mass models of ARIS (all without umbilicals). Direct and indirect disturbances were applied to these three models, and the responses were compared.

The linearized reduced-mass model presented in this TM captures the significant system rigid-body dynamics of the high-fidelity, nonlinear model of ARIS. However, being simpler, it is more suitable for controller design while using standard controller-design tools. The relatively low level of model uncertainty could translate, in principle, into a high level of derived-controller performance.

The techniques employed in this work could be used for solving and visualizing a variety of complex, over-constrained dynamics problems that model the interactions among several rigid bodies. However, these techniques are particularly advantageous for microgravity studies, where testing a microgravity isolation system in a standard Earth-gravity environment is difficult, if not impossible. The models developed here can be used as virtual test hardware for new configurations of umbilicals and payloads.

As the *ISS* nears completion, and a full-time microgravity research program develops, it is reasonable to expect that there will be an increased emphasis on the quality of the *ISS* microgravity environment. Suitable high-fidelity models of ARIS permit the development of correspondingly high-performance controllers. Improved controllers, in turn, facilitate the provision of an improved microgravity environment for the *ISS* science community.

Part three of this series presents the incorporation of ARIS umbilicals into the ARIS model, which is the final step in the dynamical modeling process. The completed nonlinear model could be used for simulation studies or, in linearized form, for controller design using MATLAB® or other popular design tools.

REFERENCES

1. Hampton, R.D.; and Beech, G.S.: "A Kane's Dynamics Model for the Active Rack Isolation System," *NASA/ TM—2001–2110063*, 36 pp., Marshall Space Flight Center, AL, June 2001.

2. Kane, T.R.; and Levinson, D.A.: *Dynamics: Theory and Applications*, 379 pp., McGraw-Hill, Inc., New York, NY, 1985.

3. Kane, T.R.; and Levinson, D.A.: *Dynamics Online: Theory and Implementation With Autolev™*, 408 pp., Sunnyvale, CA, 1996.

4. Reckdahl, K.J.; and Mitiguy, P.C.: *Autolev 3* (*Tutorial*), 64 pp., OnLine Dynamics, Inc., Sunnyvale, CA, March 1996.

5. *ENVISION (R) User Manual and Tutorials*, DELMIA Corporation, Troy, MI, 447 pp.

6. Beech, G.S.: *A High Fidelity Model for the Active Rack Isolation System*, Masters Thesis, 69 pp., The University of Alabama in Huntsville, Huntsville, AL, 2001.

REPORT DOCUMENTATION PAGE

Form Approved
OMB No. 0704-0188

1. AGENCY USE ONLY *(Leave Blank)*	2. REPORT DATE	3. REPORT TYPE AND DATES COVERED
	November 2004	Technical Memorandum

4. TITLE AND SUBTITLE
A "Kane's Dynamics" Model for the Active Rack Isolation System
Part Two: Nonlinear Model Development, Verification, and Simplification

5. FUNDING NUMBERS

6. AUTHORS
G.S. Beech, R.D. Hampton,* J.K. Rupert**

7. PERFORMING ORGANIZATION NAME(S) AND ADDRESS(ES)
George C. Marshall Space Flight Center
Marshall Space Flight Center, AL 35812

8. PERFORMING ORGANIZATION REPORT NUMBER
M–1126

9. SPONSORING/MONITORING AGENCY NAME(S) AND ADDRESS(ES)
National Aeronautics and Space Administration
Washington, DC 20546–0001

10. SPONSORING/MONITORING AGENCY REPO NUMBER
NASA/TM—2004–213552

11. SUPPLEMENTARY NOTES
Prepared by the Engineering Systems Department, Engineering Directorate
*United States Military Academy, **Dynetics, Inc.

12a. DISTRIBUTION/AVAILABILITY STATEMENT
Unclassified-Unlimited
Subject Category 31
Availability: NASA CASI 301–621–0390

12b. DISTRIBUTION CODE

13. ABSTRACT *(Maximum 200 words)*

Many microgravity space-science experiments require vibratory acceleration levels that are unachievable without active isolation. The Boeing Corporation's active rack isolation system (ARIS) employs a novel combination of magnetic actuation and mechanical linkages to address these isolation requirements on the *International Space Station*.

Effective model-based vibration isolation requires: (1) An isolation device, (2) an adequate dynamic; i.e., mathematical, model of that isolator, and (3) a suitable, corresponding controller. This Technical Memorandum documents the validation of that high-fidelity dynamic model of ARIS.

The verification of this dynamics model was achieved by utilizing two commercial off-the-shelf (COTS) software tools: Deneb's ENVISION®, and Online Dynamics' Autolev™. ENVISION is a robotics software package developed for the automotive industry that employs three-dimensional computer-aided design models to facilitate both forward and inverse kinematics analyses. Autolev is a DOS-based interpreter designed, in general, to solve vector-based mathematical problems and specifically to solve dynamics problems using Kane's method.

The simplification of this model was achieved using the small-angle theorem for the joint angle of the ARIS actuators. This simplification has a profound effect on the overall complexity of the closed-form solution while yielding a closed-form solution easily employed using COTS control hardware.

14. SUBJECT TERMS
ARIS, dynamics, control, math model.

15. NUMBER OF PAGES
32

16. PRICE CODE

17. SECURITY CLASSIFICATION OF REPORT	18. SECURITY CLASSIFICATION OF THIS PAGE	19. SECURITY CLASSIFICATION OF ABSTRACT	20. LIMITATION OF ABSTRACT
Unclassified	Unclassified	Unclassified	Unlimited